



**HAL**  
open science

# Weakened interannual Tropical Atlantic variability in CMIP6 historical simulations

Laura Sobral Verona, Paulo Silva, Ilana Wainer, Myriam Khodri

► **To cite this version:**

Laura Sobral Verona, Paulo Silva, Ilana Wainer, Myriam Khodri. Weakened interannual Tropical Atlantic variability in CMIP6 historical simulations. *Climate Dynamics*, 2023, 10.1007/s00382-023-06696-9 . hal-04004609

**HAL Id: hal-04004609**

**<https://hal.science/hal-04004609v1>**

Submitted on 6 Jan 2025

**HAL** is a multi-disciplinary open access archive for the deposit and dissemination of scientific research documents, whether they are published or not. The documents may come from teaching and research institutions in France or abroad, or from public or private research centers.

L'archive ouverte pluridisciplinaire **HAL**, est destinée au dépôt et à la diffusion de documents scientifiques de niveau recherche, publiés ou non, émanant des établissements d'enseignement et de recherche français ou étrangers, des laboratoires publics ou privés.



Distributed under a Creative Commons Attribution 4.0 International License

# Weakened Interannual Variability in the Tropical Atlantic

Laura Sobral Verona (✉ [verona.laura@usp.br](mailto:verona.laura@usp.br))

University of Sao Paulo: Universidade de Sao Paulo <https://orcid.org/0000-0002-7565-2009>

Paulo Silva

University of Sao Paulo: Universidade de Sao Paulo

Ilana Wainer

University of Sao Paulo: Universidade de Sao Paulo

Myriam Khodri

LOCEAN: Laboratoire d'Océanographie et du Climat Experimentations et Approches Numeriques

---

## Research Article

**Keywords:** Atlantic Zonal Mode, Atlantic Meridional Mode, hydroclimate, 34 ITCZ, Tropical Atlantic Variability, CMIP6

**Posted Date:** December 6th, 2021

**DOI:** <https://doi.org/10.21203/rs.3.rs-1108528/v1>

**License:**  This work is licensed under a Creative Commons Attribution 4.0 International License.

[Read Full License](#)

---

# Weakened interannual variability in the Tropical Atlantic

Laura Sobral Verona<sup>1\*†</sup>, Paulo Silva<sup>1\*†</sup>, Ilana Wainer<sup>1</sup> and Myriam Khodri<sup>2</sup>

<sup>1\*</sup>Oceanographic Institute, University of São Paulo, São Paulo, Brazil.

<sup>2</sup>LOCEAN-IPSL, Sorbonne University, Paris, France.

\*Corresponding author(s). E-mail(s): [verona.laura@usp.br](mailto:verona.laura@usp.br);  
[paulo2.silva@usp.br](mailto:paulo2.silva@usp.br);

Contributing authors: [wainer@usp.br](mailto:wainer@usp.br); [mkhodri@gmail.com](mailto:mkhodri@gmail.com) ;

†These authors contributed equally to this work.

## Abstract

Climate variability in the Tropical Atlantic is complex with strong ocean-atmosphere coupling, where the sea surface temperature (SST) variability impacts the hydroclimate of the surrounding continents. We observe a decrease in the variability of the Tropical Atlantic after 1970 in both CMIP6 models and observations. Most of the Tropical Atlantic interannual variability is explained by its equatorial (Atlantic Zonal Mode, AZM) and meridional (Atlantic Meridional Mode, AMM) modes of variability. The observed wind relaxation after 1970 in both the equatorial and Tropical North Atlantic (TNA) plays a role in the decreased variability. Concerning the AZM, a widespread warming trend is observed in the equatorial Atlantic accompanied by a weakening trend of the trade winds. This drives a weakening in the Bjerknes Feedback by deepening the thermocline in the eastern equatorial Atlantic and increasing the thermal damping. Even though individually the TNA and Tropical South Atlantic (TSA) show increased variability, the observed asymmetric warming in the Tropical Atlantic and relaxed northeast trade winds after the 70s play a role in decreasing the AMM variability. This configuration leads to positive Wind-Evaporation-SST (WES) feedback, increasing further the TNA SST, preventing AMM from changing phases as before 1970. Associated with it, the African Sahel shows a positive precipitation trend and the Intertropical Convergence Zone tends to shift northward, which acts on maintaining the increased precipitation.

**Keywords:** Atlantic Zonal Mode, Atlantic Meridional Mode, hydroclimate, ITCZ, Tropical Atlantic Variability, CMIP6

# 1 Introduction

Climate variability in the Tropical Atlantic region is complex and significantly different from that in the Pacific. It is not dominated by a single mode of variability like the El Niño-Southern Oscillation (ENSO) in the tropical Pacific, but instead different mechanisms with similar importance are at play (Sutton et al, 2000). Sea surface temperature (SST) variability in this region has important impacts on the climate of the surrounding continents (Lübbecke et al, 2018), influencing the meridional displacement of the Intertropical Convergence Zone (ITCZ) and the hydrological cycle (Carton et al, 1996; Giannini et al, 2003; Back and Bretherton, 2009; Tokinaga and Xie, 2011), hurricane activity (Vimont and Kossin, 2007; Patricola et al, 2014; Zhang et al, 2017) as well as impacting the marine ecosystems and fish availability (Binet et al, 2001; Subramaniam et al, 2013). A strong ocean-atmosphere coupling is present, where ocean currents, upwelling, and SST patterns are linked to pressure systems and the onset of the West African Monsoon (Cabos et al, 2019) and Northeast Brazil (NEB) precipitation (Nobre and Shukla, 1996).

The main modes of interannual variability in the Tropical Atlantic are the equatorial (zonal) and meridional modes, represented by the first two empirical orthogonal functions (EOFs) of detrended SST anomalies (Deser et al, 2010). The Atlantic Zonal Mode (AZM) or Atlantic Niño is an equatorial zonal mode akin to the Pacific El Niño, which is characterized by an equatorial cold tongue with typical SST amplitude of approximately  $0.5^{\circ}\text{C}$ , frequency of 2-3 years and the strongest amplitude during June, July and August (JJA) (Zebiak, 1993; Deser et al, 2010). However, unlike its Pacific counterpart, this mode has been suggested to be a modulation of the seasonal cycle (Burls et al, 2012), as well as being more concentrated around the equator and in the eastern side of the basin than the ENSO (Zebiak, 1993).

The dynamics underlying the Atlantic Zonal Mode is in parts similar to that of the Pacific El Niño (Ding et al, 2010), so that the Bjerknes Feedback (Bjerknes, 1969) observed in the Tropical Pacific is also present in the Tropical Atlantic (Keenlyside and Latif, 2007). In its positive phase, anomalous warming in the eastern Atlantic coupled with weaker trade winds is associated with anomalous eastward currents bringing warmer waters from the west as well as weaker upwelling in the eastern equatorial region and deeper thermocline, which combined act to enhance the initial positive anomaly, closing the feedback cycle (Bjerknes, 1969; Chang et al, 2006; Keenlyside and Latif, 2007; Deppenmeier et al, 2016; Dippe et al, 2019; Silva et al, 2021). The opposite happens in its negative phase.

On the other hand, although ocean dynamics is essential to explain the equatorial SST variations, air-sea fluxes control the off-equatorial SST anomalies for the AZM (Martín-Rey et al, 2019). Other mechanisms have also been discussed to generate the equatorial Atlantic SST variability, besides the Bjerknes Feedback, for example, the role of equatorward advection of north tropical Atlantic subsurface temperature anomalies (Richter et al, 2013) and equatorial deep jets (Brandt et al, 2011). It has also been discussed that a large part

of the variability of this mode is due to thermodynamic processes ( $68\pm 23\%$  of the variance) (Nnamchi et al, 2015), but other studies (e.g. Lübbecke et al, 2018, and references therein) conclude that despite the significant contribution of thermodynamics to the variability, the dynamics and in particular the Bjerknes Feedback plays the main role.

The AZM is tightly coupled to West African rainfall variability. The leading EOF of precipitation during JJA displays an anomaly pattern that is the strongest along the northern coast of the Gulf of Guinea (Chang et al, 2006). A warming in the equatorial Atlantic in this season leads to a weaker West African Monsoon by decreasing the sea level pressure gradient between the equator and the Saharan heat low (Losada et al, 2010). A decrease in rainfall variability over the coast of Guinea has also been associated with a weakening of the zonal mode (Tokinaga and Xie, 2011).

The second mode of Atlantic SST variability is known as the Atlantic Meridional Mode (AMM). It is represented by an interhemispheric dipole pattern characterized by cross-equatorial SST anomaly gradient, whose nodal line is displaced slightly north of the equator (Servain, 1991; Xie and Carton, 2004; Chang et al, 2006; Doi et al, 2009; Cabos et al, 2019). Its strongest amplitude occurs during the equatorial warm season (March, April and May, MAM) with SST anomalies of 0.3 to 0.5°C in the subtropics (Carton et al, 1996; Xie and Carton, 2004; Deser et al, 2010; Cabos et al, 2019). This mode show variability from interannual to decadal scales (Carton et al, 1996; Chang et al, 1997; Amaya et al, 2017). The meridional SST gradient is also connected to the ITCZ displacement into the warmer hemisphere, therefore affecting the precipitation pattern over South America, in particular in NEB (Nobre and Shukla, 1996; Xie and Carton, 2004; Chang et al, 2006; Deser et al, 2010).

The AMM shows pronounced coupling of the ocean-atmosphere through thermodynamic feedbacks (Carton et al, 1996). An anomalous cross-equatorial SST gradient pointing north drives a southwesterly surface wind anomaly reducing the predominant trade winds over the warmer region (the northern Tropical Atlantic). This decreases the evaporative cooling at the surface, causing it to warmer further (Chang et al, 1997; Chiang and Vimont, 2004; Mahajan et al, 2010; Amaya et al, 2017). In contrast, the other pole shows surface cooling, related to trade winds intensification. The SST changes are linked to changes in surface heat fluxes, characterizing a positive wind-evaporation-SST (WES) feedback (Xie and Philander, 1994; Chang et al, 1997, 2006; Amaya et al, 2017) that acts to reinforce the anomalous cross-equatorial SST gradient. In addition, results from satellite analysis during a strong AMM event in 2009 point to the importance of the wind-induced upwelling that could also act as positive feedback by further increasing the SST gradient (Foltz et al, 2012). While the WES positive feedback preferentially amplifies the meridional SST gradient, the Bjerknes Feedback is the dynamical mechanism counteracting the thermodynamic air-sea feedback (Chang et al, 2006; Deser et al, 2010).

124 Some studies have addressed changes in Atlantic SST variability that could  
125 be related to mean state changes and weakening of the feedback mechanisms.  
126 It has been shown that the interannual variability of Atlantic SST zonal gra-  
127 dient has decreased by  $48 \pm 13(11)\%$  in variance for 1960-1999 (Tokinaga and  
128 Xie, 2011). This indicates a significant weakening of the AZM due to a weaker  
129 Bjerknes Feedback related to mean state changes. A decrease in variability of  
130 the AZM after 2000 has also been linked to a weakening in the Bjerknes Feed-  
131 back due to weaker thermocline feedback and stronger thermal damping (Silva  
132 et al, 2021). Results presented in (Prigent et al, 2020) agree with the AZM  
133 weakening by showing a decrease of more than 30% in the eastern equatorial  
134 Atlantic SST variability during March, June and July between 1982-1999 and  
135 2000-2017. The Bjerknes Feedback is also pointed to have weakened after 2000  
136 together with an increased net heat flux damping (Prigent et al, 2020).

137 It has been suggested that changes in the equatorial Atlantic SST vari-  
138 ability might be related to changes in the Atlantic Meridional Overturning  
139 Circulation (AMOC) associated with the Atlantic Multidecadal Oscillation  
140 (AMO) (Prigent et al, 2020). An increase in the equatorial Atlantic SST vari-  
141 ability has been shown during AMO negative phase, related to an increase in  
142 the AZM amplitude of about 120% compared to positive AMO (Martín-Rey  
143 et al, 2018). It is hypothesized (Prigent et al, 2020) that the change in AMO  
144 phase at the beginning of 1990 from negative to positive might have played  
145 a role in the AZM variance decrease after the 2000s. Conversely, it has also  
146 been argued that there is no significant correlation between AMO and SST  
147 equatorial variability, at least from 1900 to 2000 (Tokinaga and Xie, 2011).  
148 The authors suggest instead a relation to the hemisphere asymmetric cooling  
149 effect from anthropogenic aerosols that causes weakening in the meridional  
150 and zonal SST gradients. It is also discussed that changes in the amplitude  
151 and strength of the surface wind associated with the AMM development could  
152 modulate the equatorial SST, which would also affect the AZM (Martín-Rey  
153 and Lazar, 2019).

154 Mean state changes in the Tropical Atlantic could play an important role in  
155 the variability modes. It has been shown that the Tropical Atlantic SST posi-  
156 tive trend since the 1950s plays a role in the decrease in the AZM variability  
157 (Tokinaga and Xie, 2011). On the other hand, recently a lack of surface warm-  
158 ing has been identified in the Atlantic cold tongue from 1979 to 2018, which  
159 has been linked to decreased wind stress forcing and subsequent thermocline  
160 shoaling (Nnamchi et al, 2020). This agrees with results shown in (Prigent  
161 et al, 2020) that also observe significant warming from 1982-1999 to 2000-2017  
162 mainly north of the equator, but not in the eastern equatorial Atlantic. In this  
163 study, we aim to understand how the Tropical Atlantic SST leading modes of  
164 variability changed since the beginning of XX century and the related changes  
165 in the precipitation over South America and Africa in the CMIP6 models and  
166 observations.

## 2 Methods

### 2.1 Observations and reanalysis

As reference data sets for SST, we use the NOAA Extended Reconstruction Sea Surface Temperature version 5 (ERSSTv5) (Huang et al, 2017), available from 1854-2014. We also use the monthly precipitation analysis of the Global Precipitation Climatology Project (GPCP) (Adler et al, 2018) (1979-2014) and surface wind stress from the NCEP Climate Forecast System Reanalysis (CFSR) (Saha et al, 2010).

### 2.2 Models

We use monthly single-member historical simulations from 37 models of the Coupled Model Intercomparison Project Phase 6 (CMIP6) (Eyring et al, 2016), that were available to us at the time of this analysis, for the period ranging from 1900 to 2015. These simulations are forced with common data sets that are largely based on observations. These include evolving, externally imposed forcings such as solar variability, volcanic aerosols, and changes in atmospheric composition (greenhouse gases and aerosols) caused by human activities. The data is available in the Earth System Grid Federation (ESGF) website.

In this study, a multimodel framework is used in which one ensemble member from each of 37 models is chosen. The models and ensemble members used are summarized in Table 1. All model outputs were remapped to a  $1^\circ \times 1^\circ$  horizontal resolution before the analyses.

### 2.3 Data Analysis

We estimate the Tropical Atlantic variability modes AZM and AMM based on index-driven metrics, that assumes the pole of variability does not change its position. As in (Tokinaga and Xie, 2011) the AZM is represented by an equatorial zonal SST difference index defined as the difference between the averaged SST anomaly over the ATL3 region ( $3^\circ\text{N}$ - $3^\circ\text{S}$ ,  $20^\circ\text{W}$ - $0^\circ$ , (Zebiak, 1993)) and WATL region ( $3^\circ\text{N}$ - $3^\circ\text{S}$ ,  $25^\circ\text{W}$ - $45^\circ\text{W}$ ), defined in Fig. 1a. This index, hereafter referred to as AZM, is highly correlated ( $r=+0.93$ ) with the Atlantic Niño index defined by the ATL3 region (Tokinaga and Xie, 2011). The AMM is defined as the difference between the SST anomaly average of Tropical North Atlantic (TNA,  $15^\circ\text{N}$ - $5^\circ\text{N}$  and  $50^\circ\text{W}$ - $20^\circ\text{W}$ ) and Tropical South Atlantic (TSA,  $5^\circ\text{S}$ - $15^\circ\text{S}$  and  $20^\circ\text{W}$ - $10^\circ\text{E}$ ) as defined in (Doi et al, 2009), illustrated in Fig. 1b. The spatial patterns of both modes are acquired by regressing the index into SST anomaly field. To evaluate changes in the mode's long-term variability, we compute a 31-year moving standard deviation of the index series.

The ITCZ position proxy is estimated as in (Pontes et al, 2020b). It is a position index based on weighted mean latitude where precipitation is greater than 50% of its maximum in the zonal mean. Double-ITCZ biases may be included if the associated precipitation is greater than 50% of the considered

6 *Weakened interannual variability in the Tropical Atlantic*

207 maximum (Pontes et al, 2020b). We considered the ITCZ position over the  
 208 Tropical Atlantic for the average from 40°W to 20°W.

209 All CMIP6 results are shown for the multimodel mean (MMM) of the  
 210 37 models (Table 1) with 90% confidence interval. We consider at least 60%  
 211 agreement among CMIP models. For the linear trends, we consider the MMM  
 212 significant where at least 60% of the models are significant, at least at the 90%  
 213 level.

Models	Ens. Member	Institution	Reference
ACCESS-CM2	r1i1p1f1	CSIRO-ARCCSS	Kiss et al (2020)
ACCESS-ESM1-5	r1i1p1f1	CSIRO	Ziehn et al (2020)
AWI-CM-1-1-MR	r1i1p1f1	AWI	Semmler et al (2018)
AWI-ESM-1-1-LR	r1i1p1f1	AWI	Contzen et al (2021)
BCC-CSM2-MR	r1i1p1f1	BCC	Wu et al (2019)
BCC-ESM1	r1i1p1f1	BCC	Xiao-Ge et al (2019)
CESM2	r1i1p1f1	NCAR	Lauritzen et al (2018)
CESM2-WACCM	r1i1p1f1	NCAR	Liu et al (2018)
CIesm	r1i1p1f1	THU	Lin et al (2020)
CMCC-CM2-HR4	r1i1p1f1	CMCC	Cherchi et al (2019)
CMCC-CM2-SR5	r1i1p1f1	CMCC	Cherchi et al (2019)
CMCC-ESM2	r1i1p1f1	CMCC	Cherchi et al (2019)
CNRM-CM6-1	r1i1p1f2	CNRM-CERFACS	Volodire et al (2019)
CNRM-CM6-1-HR	r1i1p1f2	CNRM-CERFACS	Volodire et al (2019)
CNRM-ESM2-1	r1i1p1f2	CNRM-CERFACS	Séférian et al (2019)
CanESM5	r1i1p1f1	CCCma	Swart et al (2019)
CanESM5-CanOE	r1i1p2f1	CCCma	Swart et al (2019)
E3SM-1-0	r1i1p1f1	E3SM-Project	Golaz et al (2019)
E3SM-1-1	r1i1p1f1	E3SM-Project	Golaz et al (2019)
E3SM-1-1-ECA	r1i1p1f1	E3SM-Project	Burrows et al (2020)
EC-Earth3	r1i1p1f1	EC-Earth-Consortium	Wyser et al (2020)
EC-Earth3-AerChem	r1i1p1f1	EC-Earth-Consortium	Döscher et al (2021)
EC-Earth3-CC	r1i1p1f1	EC-Earth-Consortium	Döscher et al (2021)
EC-Earth3-Veg	r1i1p1f1	EC-Earth-Consortium	Wyser et al (2020)
EC-Earth3-Veg-LR	r1i1p1f1	EC-Earth-Consortium	Döscher et al (2021)
FGOALS-g3	r1i1p1f1	CAS	Li et al (2020)
GISS-E2-1-G	r1i1p1f1	NASA-GISS	Kelley et al (2020)
GISS-E2-1-H	r1i1p1f1	NASA-GISS	Kelley et al (2020)
INM-CM5-0	r1i1p1f1	INM	Volodin et al (2019)
IPSL-CM6A-LR	r1i1p1f1	IPSL	Boucher et al (2020)
IPSL-CM6A-LR-INCA	r1i1p1f1	IPSL	Boucher et al (2020)
MPI-ESM-1-2-HAM	r1i1p1f1	HAMMOZ-Consortium	Tegen et al (2019)
MPI-ESM1-2-HR	r1i1p1f1	DKRZ	Müller et al (2018)
NorCPM1	r1i1p1f1	NCC	Bethke et al (2021)
NorESM2-LM	r1i1p1f1	NCC	Seland et al (2020)
NorESM2-MM	r1i1p1f1	NCC	Seland et al (2020)
UKESM1-0-LL	r1i1p1f2	MOHC	Sellar et al (2019)

**Table 1** Models and the respective ensemble members used. The letters *r*, *i*, *p* and *f* stand for *realization*, *initialization method*, *physics* and *forcing*, respectively.

214 **3 Results**

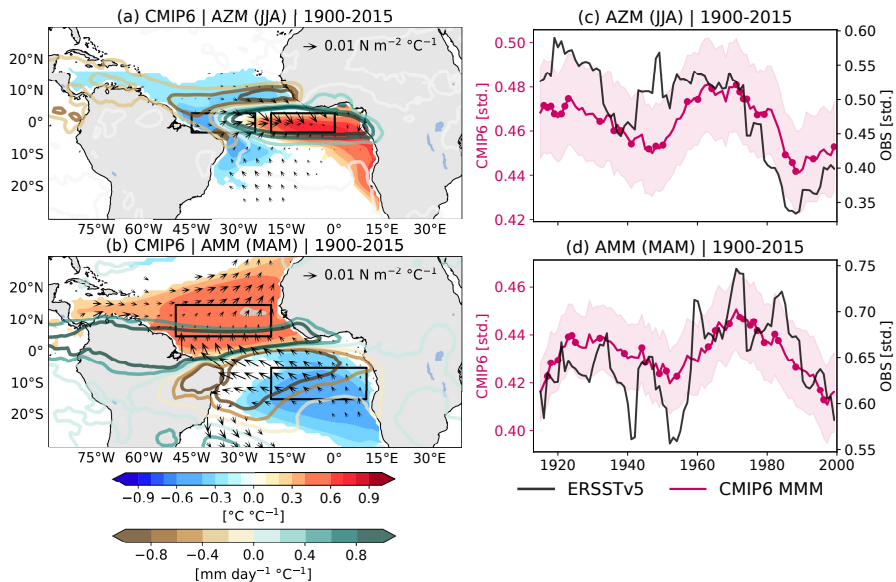
215 The majority of the CMIP6 models represent the Tropical Atlantic variability  
 216 modes pattern, as shown by the map of significant correlations at the 95%

217 level for at least 60% of the models (Fig. 1a and b). The AZM is defined by the  
218 characteristic warm region on the eastern equatorial Atlantic (Xie and Carton,  
219 2004; Deser et al, 2010). It also shows a negative SST anomaly that surrounds  
220 the equatorial warm tongue. The AMM typical pattern is also represented  
221 by the CMIP6 MMM, which shows a positive SST gradient pointing to the  
222 Northern Hemisphere (Xie and Carton, 2004; Amaya et al, 2017; Deser et al,  
223 2010). The wind pattern points to the warmer region for both modes. This  
224 means a wind relaxation in the equatorial region for the positive phase of the  
225 AZM and over the warm pole of the AMM (Xie and Carton, 2004; Deser et al,  
226 2010; Amaya et al, 2017; Silva et al, 2021).

227 Although some equatorial Atlantic SST and wind biases still show the  
228 same pattern as in previous model generations (Richter and Xie, 2008), results  
229 from Richter and Tokinaga (2020) show a slight improvement in the Tropical  
230 Atlantic SST representation from CMIP5 to CMIP6 models. Despite the little  
231 improvement in the model's mean state, many CMIP6 models reproduce well  
232 the Tropical Atlantic SST variability, correctly capturing the amplitude and  
233 seasonality of both AZM and AMM (Richter and Tokinaga, 2020). In addition,  
234 it is suggested that there is a relatively weak link between mean state biases  
235 and the quality of the simulated variability (Prodhomme et al, 2019).

236 The precipitation pattern associated with each mode is also represented in  
237 Fig. 1a and b. For both modes the precipitation is associated with the warmer  
238 regions, this characterizes the precipitation pattern in the African Sahel for  
239 the AZM (Chang et al, 2006; Deser et al, 2010). The AMM is mostly related to  
240 the precipitation pattern in the NEB and Amazon (Nobre and Shukla, 1996;  
241 Deser et al, 2010). The resultant precipitation pattern is connected also to  
242 the ITCZ displacement into the warmer hemisphere (Nobre and Shukla, 1996;  
243 Chiang et al, 2002).

244 After 1970, the AZM and AMM present a decrease in variability, shown by  
245 the 31-year moving standard deviation in Fig. 1c and d. The CMIP6 MMM  
246 agrees with ERSSTv5 data set. The reduction in variability for the AZM has  
247 already been identified for observations from 1960 to 1999 (Tokinaga and Xie,  
248 2011). Furthermore, the AZM weakening has also been shown after the 2000s  
249 in observations and reanalyses (Prigent et al, 2020) and for an ensemble of  
250 7 reanalyses products (Silva et al, 2021). The AZM variability reduction is  
251 related to the Bjerkens Feedback weakening due to weaker thermocline feed-  
252 back (Tokinaga and Xie, 2011) and stronger thermal damping (Silva et al,  
253 2021), with the main contribution from the increased latent heat flux (Pri-  
254 gent et al, 2020). There is a strong coupling between the wind pattern and the  
255 Tropical Atlantic SST gradients. The weakened Bjerknes Feedback is identified  
256 to be responsible for the decrease in the AZM variability, in connection to a  
257 relaxation of the trade winds (Tokinaga and Xie, 2011), as well as its changes  
258 in response to the SST anomalies (Prigent et al, 2020).

8 *Weakened interannual variability in the Tropical Atlantic*

**Fig. 1** Spatial pattern of the Tropical Atlantic variability modes (a) AZM for JJA and (b) AMM for MAM from 1900 to 2015. Shading represents the index correlation for the SST anomaly ( $^{\circ}\text{C }^{\circ}\text{C}^{-1}$ ) and the contour lines represent the index regressed against precipitation anomaly ( $\text{mm day}^{-1} \text{ }^{\circ}\text{C}^{-1}$ ), both only shown for regions where correlations are significant at the 95% for at least 60% of the models. Vectors represent wind stress anomaly regressed against each mode index ( $\text{N m}^{-2} \text{ }^{\circ}\text{C}^{-1}$ ), only shown where at least one of the wind components present significant correlation at 95% for at least 60% of the models. The black delimited boxes represent regions used for the index calculation (see Section 2). (c) and (d) 31-year running standard deviation for each mode for ERSSTv5 and for CMIP6 MMM. Shading indicates the 90% confidence interval for the MMM. Dots indicate where at least 60% of the models agree on the sign of the 1<sup>st</sup> derivative

259 To better understand the annual variability of each mode for the SST and  
 260 the related wind stress pattern, we compute the annual cycle of the regression  
 261 of surface wind stress and SST anomalies against the AZM index in JJA (in  
 262 the zonal section between  $40^{\circ}\text{W}$ - $10^{\circ}\text{E}$  averaged over  $4^{\circ}\text{N}$ - $4^{\circ}\text{S}$ , box **a** in Fig. 2d)  
 263 and the AMM index in MAM (in the meridional section between  $15^{\circ}\text{S}$ - $15^{\circ}\text{N}$   
 264 averaged over  $25^{\circ}\text{W}$ - $15^{\circ}\text{W}$ , box **b** in Fig. 2d). The results are shown in Figs.  
 265 2a and b, respectively.

266 The mode's annual variability is well represented by the CMIP6 MMM,  
 267 as shown in Fig. 2. As it is observed in Fig. 2a, the AZM pattern in the SST  
 268 becomes evident in JJA, with a zonal dipole with high positive correlations  
 269 in the east and negative in the west. The AZM for the CMIP6 MMM shows  
 270 greater variability during JJA, a delay of one month compared to the ERSSTv5  
 271 data set that represents the greatest AZM variability during MJJ (Fig. 2c).  
 272 Deser et al (2010) show AZM the highest variability during MJJ obtained  
 273 from the first empirical orthogonal function based on HadISST data set during  
 274 1900–2008. For the CMIP6 and CMIP5 data sets, Richter and Tokinaga (2020)

275 also show a small delay in the variability of the zonal mode compared to ERA-  
276 5 reanalysis. As the ERSSTv5, the ERA-5 standard deviation peaks in June,  
277 while for the CMIP6 and CMIP5 MMM the peak occurs one month later, as  
278 shown here, during July. As observed in Fig. 2c, there is a large similarity  
279 between the magnitude of the zonal mode's variability represented by the  
280 CMIP6 MMM and ERSSTv5.

281 A strong positive correlation with zonal wind stress is observed in the  
282 preceding season (MAM), which suggests that the variability of the AZM is  
283 influenced by the variability of surface winds in the western side of the basin  
284 one season before. This is consistent with the observed positive correlation  
285 between MAM wind stress in the western equatorial Atlantic and SST vari-  
286 ability in JJA in the eastern side (Richter et al, 2013). This peak in wind  
287 variability is delayed by one month in the CMIP6 models (peak in May Fig.  
288 2c) when compared to the ERA-5 reanalysis (peak in April), although this  
289 does not change the peak in variability in MAM (Richter and Tokinaga, 2020).

290 For the AMM (Fig. 2c) the greatest variability in ERSSTv5 occurs during  
291 MAM, agreeing with Deser et al (2010). However, this peak is not as clear  
292 as that observed for the AZM in JJA. The CMIP6 does not represent as well  
293 the climatological change in monthly variability for the AMM. The standard  
294 deviation from January to June is almost the same, after that there is a slight  
295 decrease in variability. The spatial SST pattern of the AMM appears in MAM  
296 for the CMIP6 MMM (Fig. 2b). Richter and Xie (2008) point that the zonal  
297 wind variability peaks one month earlier (January) than the SST (February),  
298 which is consistent with the forcing of AMM variability by trade wind vari-  
299 ations. There is not a clear lag between the wind and the SST pattern in  
300 the northern Tropical Atlantic in our results; however, a region of negative  
301 correlations starts to develop in JJA between 0° and 5°S, which could be  
302 explained by the WES feedback, being a result of the wind forcing observed  
303 in the preceding season.

304 The AMM is dominated by the TNA variability (Amaya et al, 2017), thus  
305 looking only at the northern pole, the AMM variability in ERA-5 is highest  
306 from February through May (Richter and Tokinaga, 2020), similar to that  
307 represented by ERSSTv5 (Fig. 2c). However, as shown in Fig. 2c, the CMIP6  
308 AMM variability underestimates that of ERSSTv5. Similarly, it has also been  
309 found that AMM variability represented by CMIP6 underestimates that of  
310 ERA-5 (Richter and Tokinaga, 2020). The authors suggest this to be related  
311 to biases in the mixed layer depth in CMIP models.

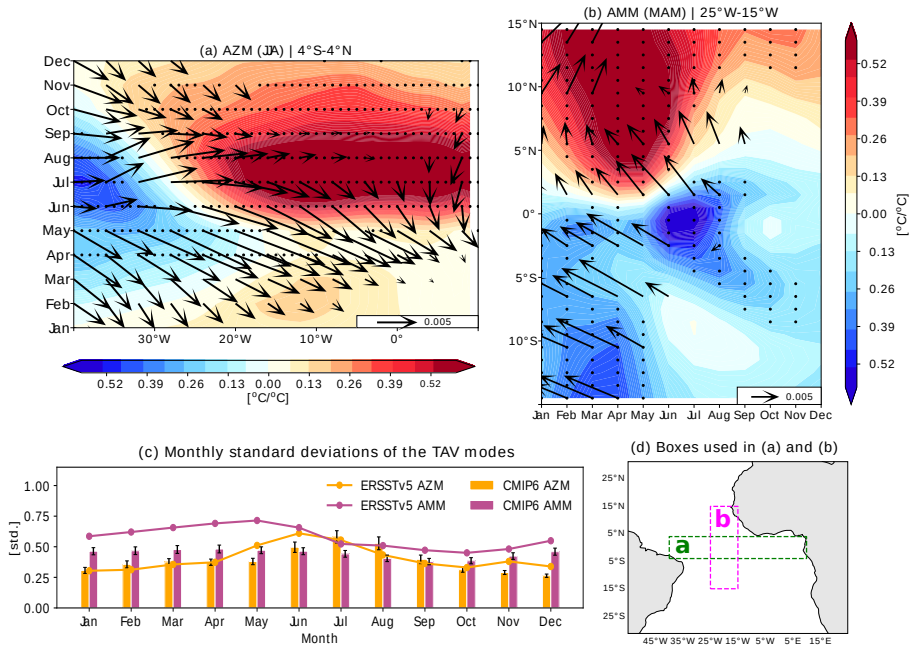


**Fig. 2** (a) Regression of annual Tropical Atlantic variability modes index against SST and wind stress anomalies for each calendar month. Stippling indicates regions where correlations are significant at the 95% level for at least 60% of the models. Vectors are shown only where the correlations are significant at the 95% for at least 60% of the models, for at least one of the wind components. In (a) AZM (JJA) we use the meridional mean in  $4^{\circ}\text{N}$ - $4^{\circ}\text{S}$  and in (b) AMM (MAM) we use the zonal mean in  $25^{\circ}\text{W}$ - $15^{\circ}\text{W}$ . Vector units in (a) and (b) are  $\text{N m}^{-2} \text{ } ^{\circ}\text{C}^{-1}$ . (c) Monthly standard deviations of the AZM and AMM modes for ERSSTv5 and for CMIP6 MMM with 90% confidence interval. All results are for the period of 1900 to 2015. (d) Boxes used in (a) and (b)

312 Given the clear relation between wind stress and the Tropical Atlantic  
 313 SST pattern shown in Fig. 2a and b, we look for changes that could explain  
 314 the decrease in the variability of the modes. For the wind pattern related to  
 315 the AZM we use box 1 in Fig. 3a that presents winds from the southeast in  
 316 the climatology. In the anomaly time series (Fig. 3b) we observe wind stress  
 317 anomalies that are typically from the southeast up to 1970, then the anomalies  
 318 reverse to the northwest from 1970 to 2000, and after that, the anomalies  
 319 start to rotate to the south again. This period from 1970 to 2000 where the  
 320 wind over the AZM region relaxes (northwest anomalies) is consistent with  
 321 the period that we observe the reduction in the long-term variability (Fig.  
 322 1c). The weakening of the trade winds has been suggested to be related to  
 323 the AZM decrease in variability in connection with deepening of thermocline  
 324 and intensified warming in the eastern equatorial Atlantic (Tokinaga and Xie,  
 325 2011), weaker thermocline feedback, and stronger thermal damping (Silva et al,  
 326 2021). The increase in the thermal damping seems to lead the Tropical Atlantic  
 327 SST changes (Prigent et al, 2020).

328 The same behavior is observed for the AMM, where the climatological wind  
329 pattern is from the northeast (Fig. 3a box 2), in the time series the anomalies  
330 agree with this predominant direction up to 1980. After 1980, the wind stress  
331 anomaly over the TNA also shows relaxation up to 2015, with wind stress  
332 anomalies from the southwest (Fig. 3c), the same period in which we observe  
333 a decrease in AMM variability (Fig. 1d). The wind relaxation over the TNA  
334 normally is associated with an increase in SST anomalies via positive WES  
335 feedback (Chang et al, 1997; Amaya et al, 2017). This may account for the  
336 AMM decreased variability after 1980, especially related to AMM negative  
337 phases. During these phases, the TNA shows negative SST anomalies (opposite  
338 in the TSA), the wind relaxation in this region acts in the opposite direction  
339 of the positive WES feedback. Therefore, the wind anomaly would imply a  
340 decrease in the interhemispheric SST gradient during negative phases.

341 The associated precipitation also changes its behavior during 1900 to 2015  
342 for the African Sahel (Fig. 3a box 3) and NEB (Fig. 3a box 4), in agreement  
343 with the observational data set (Fig. 3d and e). The precipitation over the Sahel  
344 increases significantly after the 1970s at the 90% level for at least 60% of the  
345 CMIP6 models. Both data sets agree on the positive trend since 1970 and 1980,  
346 respectively  $0.0037 \text{ mm day}^{-1} \text{ year}^{-1}$  for CMIP6 and  $0.0087 \text{ mm day}^{-1} \text{ year}^{-1}$   
347 for observations. The NEB time series shows a larger amplitude compared  
348 to the Sahel precipitation and presents a decrease in precipitation over time,  
349 enhanced after the 1970s. The CMIP6 models agree in the direction of the  
350 change over NEB (shown by the dots that represent the agreement in the sign  
351 of the first derivative); however, only 7 of the 37 models present a significant  
352 negative trend at the 90% level. Conversely, a decrease in precipitation over the  
353 Sahel accompanied by an increase in the equatorial West Africa and Amazon  
354 are reported in Tokinaga and Xie (2011), with similar trends observed for  
355 2000-2017 in Prigent et al (2020).

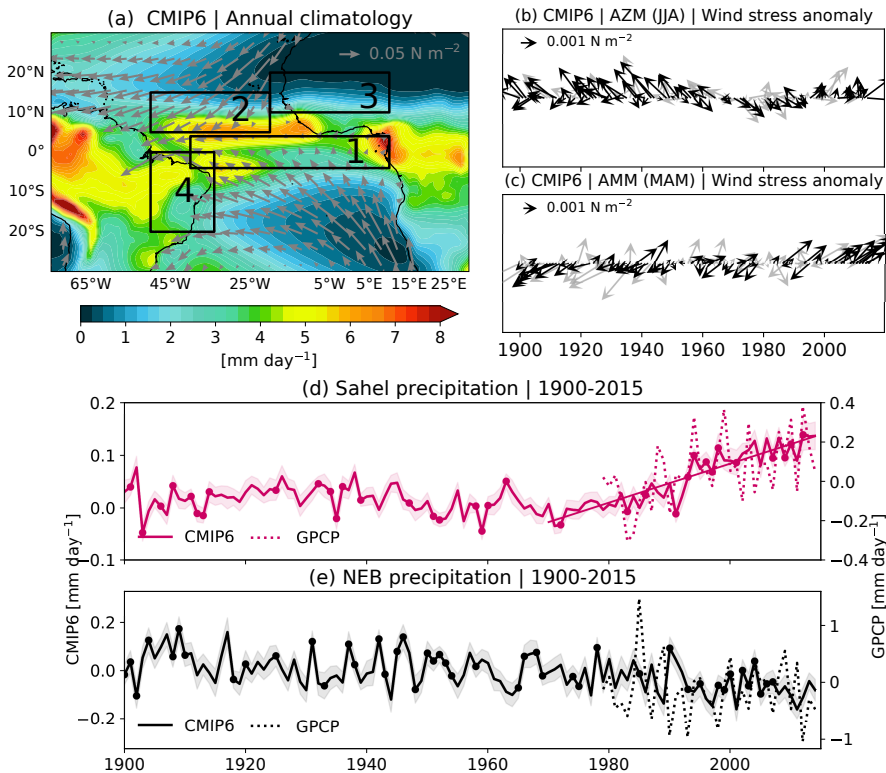


**Fig. 3** (a) CMIP6 MMM wind stress annual average for 1900 to 2015. (b) and (c) Vector time series of wind stress anomaly from 1900 to 2015 for each predominant season for the Tropical Atlantic variability modes at the black delimited boxes in (a), for AZM average between 4°N-4°S, 40°W-10°E (box 1) and for AMM mean between 5°N-15°N, 50°W-15°W (box 2). The black vectors show where 60% or more models agree on the sign for at least one of the wind stress components, for the gray arrows there is no agreement among models. The precipitation time series over (d) Sahel (box 3) and (e) NEB (box 4) for 1900 to 2015 for the CMIP6 MMM and GPCP data set. Shading indicates the 90% confidence interval for the MMM. Dots indicate where at least 60% of the models agree on the sign of the 1<sup>st</sup> derivative. In (d) the continuous line indicate the trend from 1970 (for CMIP6 MMM) and from 1980 (for GPCP) to 2015

356 Thus, the decrease in the variability of the modes appears to be related to  
 357 the long-term wind relaxation after the 1970s, which impacts the hydroclimate  
 358 associated with the South America and African continents, in particular the  
 359 NEB and Sahel regions. To investigate further, we examine the **monthly** spatial  
 360 long-term trends from 1970 to 2015 for the Tropical Atlantic SST, wind stress,  
 361 and precipitation over land (Fig. 4).

362 We show that there is a relative agreement between CMIP6 MMM and  
 363 observations trends. For both data sets, a similar pattern emerges from the  
 364 SST trend, the northern Tropical Atlantic presents a larger positive trend  
 365 ( $\sim 2 \times 10^{-2} \text{ }^\circ\text{C year}^{-1}$ ) while for the southern Atlantic the SST trend is smaller

( $\sim 0.9 \times 10^{-2} \text{ }^\circ\text{C year}^{-1}$ ). This trend after the 1970s is probably related to the regime shift around the 1980s, but with slightly different times around the world, that can represent a major change in the Earth's biophysical systems (Reid et al, 2016). From the mid-1970s onward, increased warming over the Northern Hemisphere ( $1.0^\circ\text{C}$ ) compared to  $0.6^\circ\text{C}$  in the southern basin is observed (Servain et al, 2014). The Northern Hemisphere warming also corroborates previous results that show significant MJJ warming for 2000-2017 (Prigent et al, 2020). The SST positive trend over the equatorial region contributes to the observed weakening of the AZM variability by decreasing its zonal gradient.

The increase in the Tropical Atlantic SST is associated with the increase in the variability for each pole of the AMM (TNA and TSA, Supplementary Fig. 1). The TNA warming results in its increased variability under global warming, which is influenced by an increase in ENSO variability and teleconnections (Yang et al, 2021). It is worth noting, however, that other studies (Hu et al, 2013; Lübbecke and McPhaden, 2014) identify a decrease in ENSO variability after 2000, so the link between the increase in TNA variability and ENSO is not clear. We observe warming also in the TSA after 1970, slightly smaller than the TNA (Fig. 4a,b and Supplementary Fig. 2), in association with increased variability in this region. Even though individually each pole of the AMM shows an increase in variability, the meridional asymmetric warming in the Tropical Atlantic (Fig. 4a and b) plays a role in decreasing AMM long-term variability (Fig. 1d).

The warming is associated with the southwest wind stress trend (Fig. 4a and b) located mostly over the equatorial region of the Northern Hemisphere (TNA box in Fig. 1b) for the CMIP6 MMM, which characterizes a relaxation of the northeast trade winds. Approximately the same pattern of wind relaxation is shown by the CFSR trends; however, the observational data set presents a westward trend farther north ( $\sim 15^\circ\text{N}$ ) as well as a small trend in the Southern Hemisphere ( $\sim 5^\circ\text{S}$ ). The long-term relaxation of the winds in the Northern Hemisphere is probably coupled with the increased warming in this region (Tokinaga and Xie, 2011). The intensified interhemispheric SST gradient together with the wind relaxation in the equatorial Northern Hemisphere contribute to the decrease in AMM long-term variability. The SST positive trend is reinforced by the positive WES feedback resultant from the wind relaxation, which acts on reducing the surface latent heat flux, increasing further the SST (Xie and Carton, 2004; Amaya et al, 2017). Considering the 1970-2015 trends, the configuration of increased SST and weakened winds in TNA is maintained, therefore decreasing AMM variability. The same pattern of increased SST over the Northern Hemisphere and weakening of the northeast trade winds was identified to be related to decreased AMM variability for the mid-Pliocene (Pontes et al, 2020a).

Both SST and wind stress trends can modify the precipitation in the Tropical region. CMIP6 MMM and GPCP show a positive trend in the precipitation over the Sahel. We suggest that the increased precipitation over the Sahel is

411 connected with the strong SST warming in the Northern Hemisphere, con-  
412 sidering the positive correlation between SST and precipitation found in the  
413 Tropical Atlantic, also apparent over the subtropical North Pacific (Xie et al,  
414 2010). In contrast, a positive trend in the precipitation over West Africa and  
415 Guinea coast and a negative trend over the Sahel has been shown (Tokinaga  
416 and Xie, 2011). These differences are probably related to the stronger SST  
417 positive trend over the Atlantic cold tongue region, which is not observed here.  
418 There is a positive trend for the precipitation over the Amazon only shown by  
419 the GPCP data set, which corroborates with previous results (Tokinaga and  
420 Xie, 2011). However, the CMIP6 MMM does not present any consistent trend  
421 over South America, which has been pointed to as a region of precipitation  
422 biases in CMIP models (Richter and Xie, 2008; Tian and Dong, 2020).

423 We observe a positive trend in the ITCZ position proxy based on the  
424 related precipitation pattern (Pontes et al, 2020b) of  $0.022^\circ \text{ year}^{-1}$  that is sig-  
425 nificant at the 90% level for the observations (Fig. 4c). The CMIP6 MMM  
426 also shows a significant positive trend of  $0.010^\circ \text{ year}^{-1}$  that is represented by  
427 46% of the models (17/37). It is consistent with the increased SST positive  
428 trend over the Northern Hemisphere that serves as an attractor for the ITCZ  
429 shift to the warmer region (Schneider et al, 2014; Mamalakis et al, 2021). The  
430 ITCZ northward trend explains the observed positive trend in the precipita-  
431 tion over the Sahel (Fig. 4a,b and 3d). It was expected a negative trend in the  
432 NEB precipitation, however, it was neither consistent among CMIP6 models  
433 nor for the observational data set (Fig. 3e and 4). The precipitation trend and  
434 ITCZ northward shift are also consistent with the AMM reduced variability.  
435 Given the constant anomalous warming and wind relaxation in the Northern  
436 Hemisphere related to the decreased AMM variability, the ITCZ shifts north-  
437 ward following the increased SST (Fig. 4c). As consequence, the precipitation  
438 pattern is also displaced northward, resulting in increased precipitation over  
439 the African Sahel (Fig. 4a) and decreased precipitation over the NEB (not  
440 consistent among CMIP6 models).

441 The ITCZ tends to follow the warmer oceanic region, but the results change  
442 when considering different periods and different ITCZ position proxies. A  
443 southward displacement of the ITCZ because of the intensified SST warming in  
444 the eastern equatorial Atlantic has been suggested (Tokinaga and Xie, 2011),  
445 based on the increased cloud cover over this region from 1960 to 2000. Differ-  
446 ently, using as a proxy of the ITCZ position the latitude where the meridional  
447 component of the wind stress along  $30^\circ\text{W}$  equals zero, no significant long-term  
448 change in the ITCZ position from 1964 to 2012 has been observed (Servain  
449 et al, 2014). From 2000 to 2017, an increase in precipitation over the western  
450 African coast, northeastern Brazil, and north of the equator has been detected  
451 (Prigent et al, 2020), related to the northward shift of the ITCZ position. The  
452 ITCZ trend shown here by observations and the CMIP6 MMM is consistent  
453 with the SST positive long-term trend intensified over the northern basin and  
454 the increase in Sahel precipitation.

455 The changes in Tropical Atlantic variability may be modulated by the  
456 AMO behavior during the last 50 years (Prigent et al, 2020). After the 1970s,  
457 the AMO index changes its phase from negative to positive (Frajka-Williams  
458 et al, 2017), which matches the period of decreased modes variability. During  
459 positive AMO, the AZM displays smaller amplitudes when compared to its  
460 amplitude during negative AMO (Martín-Rey et al, 2018). It is also pointed  
461 that AMO may show causal influence on the AMM on decadal time scales  
462 (Vimont and Kossin, 2007; Veiga et al, 2020). Moreno-Chamarro et al (2020)  
463 observed a link between AMOC, AMO, and ITCZ variability. The authors  
464 identified a change in AMOC's cross-equatorial heat transport that induces  
465 AMO phase change (from negative to positive). This leads to a northward  
466 ITCZ shift, as observed in our results, to compensate the energy imbalance  
467 across the hemispheres. Therefore, changes in AMOC and AMO phasing could  
468 modify AMM variability.

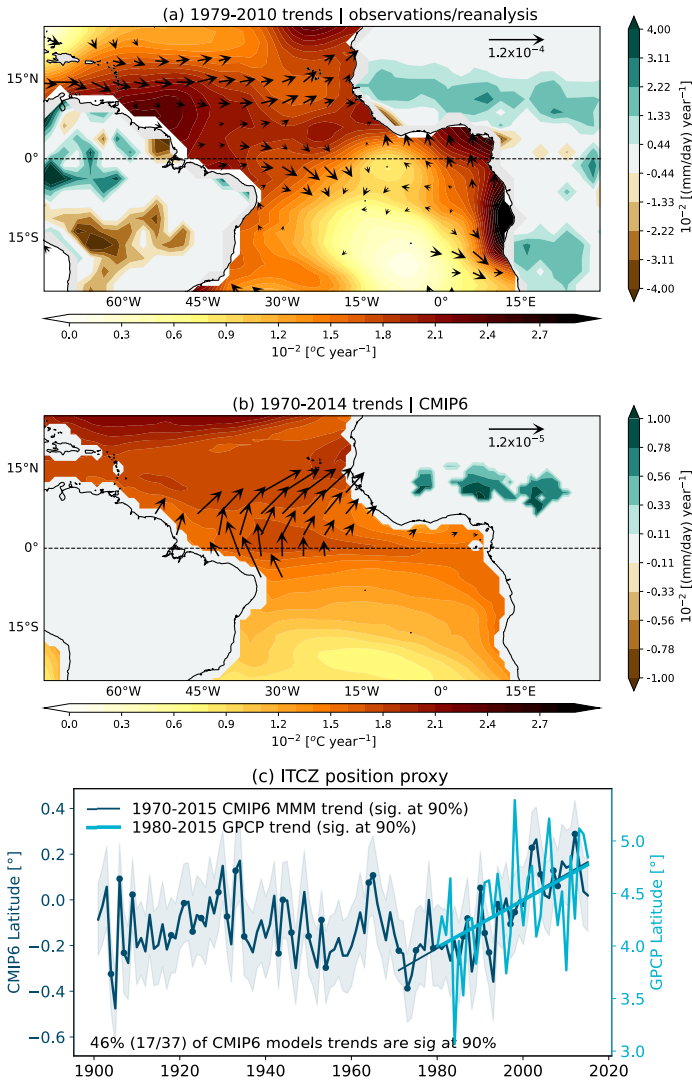


**Fig. 4** Trends for SST, wind stress and precipitation for (a) ERSSTv5, CFSR and GPCP respectively of [monthly series](#) from 1979 to 2010 and for (b) CMIP6 MMM. Trends are only shown where significant at the 95% level for observations and reanalysis and where at least 60% of the models show significant trends at the 95% level for the CMIP6 MMM. Note that (a) and (b) present different scales for precipitation and vectors. (c) ITCZ position proxy based on [annual](#) precipitation for CMIP6 MMM (dark blue) and GPCP (light blue). Shading indicates the 90% confidence interval for the CMIP6 MMM. Dots indicate where at least 60% of the models agree on the sign of the 1<sup>st</sup> derivative

469

## 4 Summary and conclusions

470

We rely on monthly historical simulations from 37 CMIP6 models ([Eyring et al, 2016](#)) as well as reconstructions and reanalyses for SST, precipitation,

471

472 and surface wind stress to investigate changes in the Tropical Atlantic modes  
473 of variability in 1900-2015 and their connection with precipitation in the sur-  
474 rounding continents. Both the AZM and AMM show a decrease in variability  
475 after 1970.

476 In agreement with Richter et al (2013), our results show a strong positive  
477 correlation between MAM zonal winds stress and the JJA time series of the  
478 AZM, suggesting that changes in wind stress variability in the preceding season  
479 could influence variability in SST in the eastern equatorial Atlantic, which  
480 peaks in JJA (Zebiak, 1993; Deser et al, 2010). For the AMM, on the other  
481 hand, we do not observe a clear lag with respect to wind stress, with the largest  
482 correlation between the mode and the wind occurring in MAM, the season  
483 when the mode peaks (Deser et al, 2010).

484 Considering the coupling of the modes with the surface wind, we observe  
485 a relaxation in both the equatorial Atlantic region and the northern Tropi-  
486 cal Atlantic after 1970. Concerning the AZM, a widespread warming trend is  
487 observed in the equatorial Atlantic, accompanied by the weakening trend of the  
488 trade winds. This resonates with other studies that discuss the weaker trades  
489 and warmer equatorial Atlantic driving a weakening in the Bjerknes Feedback  
490 by deepening the thermocline in the eastern equatorial Atlantic (Tokinaga and  
491 Xie, 2011; Silva et al, 2021). The warmer sea surface also leads to stronger  
492 thermal damping (Prigent et al, 2020; Silva et al, 2021), further weakening the  
493 Bjerknes Feedback and reducing the AZM variability.

494 Regarding the AMM, the relaxation of the northeastern trade winds con-  
495 tributes to a decrease in the amplitude of AMM negative phases by weakening  
496 the WES feedback. We identified a warming trend and increased variability  
497 for each pole, TNA and TSA, of the AMM. Yang et al (2021) suggest TNA  
498 variability is associated with global warming and increased ENSO variabil-  
499 ity, although this contrasts with other studies (e.g., Hu et al, 2013; Lübbecke  
500 and McPhaden, 2014) that show a decrease in ENSO variability after 2000.  
501 The TNA and TSA show increased variability individually, but the asymmet-  
502 ric warming associated with the northeast trade winds relaxation after 1970  
503 maintains the positive WES feedback, thus leading to weakened AMM vari-  
504 ability. This was also identified for the mid-Pliocene (Pontes et al, 2020a), an  
505 important parallel given it was a period of significantly warmer climate than  
506 at present, with similar atmospheric carbon dioxide concentrations.

507 Associated with SST and trade wind, a positive precipitation trend over the  
508 Sahel is also observed in both the simulations and the observations. Positive  
509 precipitation trends over the Amazon and negative over central South America  
510 are also present in the observations but are not significant in the CMIP6  
511 multimodel mean. The results suggest that the southwest wind anomaly in the  
512 TNA (relaxation of the northeasterly trade winds) carries more humidity into  
513 the Sahel region, resulting in positive precipitation trends. Consistent with the  
514 decreased variability in the AMM, the ITCZ tends to shift northward, which  
515 helps to maintain the increased precipitation over the African Sahel (Chiang  
516 et al, 2002; Deser et al, 2010).

517 These variability changes may be modulated by the AMO phase changing,  
518 from negative to positive, after the 1970s (Prigent et al, 2020; Frajka-  
519 Williams et al, 2017). The AMO phase change induced by AMOC's change in  
520 cross-equatorial heat transport also leads to ITCZ northward shift (Moreno-  
521 Chamarro et al, 2020), which is consistent with our results for AMM and  
522 AZM decreased variability. Further studies are needed to investigate the role  
523 of AMO or other remote mechanisms that could modulate the observed and  
524 simulated shift in Tropical Atlantic Variability in the last decades.

525 **Acknowledgments.** This study was supported in part by the Grants  
526 FAPESP (Fundação de Amparo à Pesquisa do Estado de São Paulo):  
527 2020/08490-0; 2021/04596-1; 2018/14789-9; CNPq (Conselho Nacional de  
528 Desenvolvimento Científico e Tecnológico): 301726/2013-2, 405869/20134;  
529 CNPq.MCT.INCT.CRIOSFERA 573720/2008-8, by the Coordenação de  
530 Aperfeiçoamento de Pessoal de Nível Superior - Brasil (CAPES) - Finance  
531 Code 001 and CAPES 88887.314387/2019-00. This work was undertaken in  
532 the framework of the French L-IPSL LABEX and the IPSL Climate Graduate  
533 School EUR.

## 534 **Declarations**

535 **Conflict of interest:** The authors declare that they have no conflict of  
536 interests.

537 **Authors' contributions:** LV, PS and IW designed the study. LV and PS  
538 performed the analysis and wrote the manuscript draft. All authors contributed  
539 to the interpretation of the results and to the improvement of the manuscript.

540 **Data availability:** The datasets generated during and/or analysed during  
541 the current study are available in the Earth System Grid Federation  
542 (ESGF) repository [<https://esgf-node.llnl.gov/search/cmip6/>]. Other data sets  
543 (ERSSTv5, GPCP and CFSR) are available in Climate Data Guide repository  
544 [<https://climatedataguide.ucar.edu/>].

## 545 **References**

- 546 Adler RF, Sapiano MR, Huffman GJ, et al (2018) The Global Precipitation Cli-  
547 matology Project (GPCP) monthly analysis (new version 2.3) and a review  
548 of 2017 global precipitation. *Atmosphere* 9(4):138. [https://doi.org/10.3390/  
549 atmos9040138](https://doi.org/10.3390/atmos9040138)
- 550 Amaya DJ, DeFlorio MJ, Miller AJ, et al (2017) Wes feedback and the atlantic  
551 meridional mode: Observations and cmip5 comparisons. *Climate Dynamics*  
552 49(5):1665–1679. <https://doi.org/10.1007/s00382-016-3411-1>

- 553 Back LE, Bretherton CS (2009) On the Relationship between SST Gradients,  
554 Boundary Layer Winds, and Convergence over the Tropical Oceans. *Journal*  
555 *of Climate* 22(15):4182–4196. <https://doi.org/10.1175/2009JCLI2392.1>
- 556 Bethke I, Wang Y, Counillon F, et al (2021) Norcpm1 and its contribution to  
557 cmip6 dcpp. *Geoscientific Model Development Discussions* pp 1–84. <https://doi.org/10.5194/gmd-2021-91>
- 559 Binet D, Gobert B, Maloueki L (2001) El Nino-like warm events in the  
560 Eastern Atlantic (6 N, 20 S) and fish availability from Congo to Angola  
561 (1964–1999). *Aquatic Living Resources* 14(2):99–113. [https://doi.org/10.1016/S0990-7440\(01\)01105-6](https://doi.org/10.1016/S0990-7440(01)01105-6)
- 563 Bjerknes J (1969) Atmospheric Teleconnections from the Equatorial  
564 Pacific. *Monthly Weather Review* 97(3):163–172. [https://doi.org/10.1175/1520-0493\(1969\)097%28\\$0163:ATFTEP%28\\$2.3.CO;2](https://doi.org/10.1175/1520-0493(1969)097%28$0163:ATFTEP%28$2.3.CO;2)
- 566 Boucher O, Servonnat J, Albright AL, et al (2020) Presentation and evaluation  
567 of the ipsl-cm6a-lr climate model. *Journal of Advances in Modeling Earth*  
568 *Systems* 12(7):e2019MS002,010. <https://doi.org/10.1029/2019MS002010>
- 569 Brandt P, Funk A, Hormann V, et al (2011) Interannual atmospheric variabil-  
570 ity forced by the deep equatorial Atlantic Ocean. *Nature* 473(7348):497–500.  
571 <https://doi.org/10.1038/nature10013>
- 572 Burls N, Reason CC, Penven P, et al (2012) Energetics of the tropical Atlantic  
573 zonal mode. *Journal of climate* 25(21):7442–7466. <https://doi.org/10.1175/JCLI-D-11-00602.1>
- 575 Burrows S, Maltrud M, Yang X, et al (2020) The doe e3sm v1. 1 biogeochem-  
576 istry configuration: Description and simulated ecosystem-climate responses  
577 to historical changes in forcing. *Journal of Advances in Modeling Earth*  
578 *Systems* 12(9):e2019MS001,766. <https://doi.org/10.1029/2019MS001766>
- 579 Cabos W, de la Vara A, Koseki S (2019) Tropical Atlantic variability:  
580 observations and modeling. *Atmosphere* 10(9):502. <https://doi.org/10.3390/atmos10090502>
- 582 Carton JA, Cao X, Giese BS, et al (1996) Decadal and Interannual SST  
583 Variability in the Tropical Atlantic Ocean. *Journal of Physical Oceanogra-*  
584 *phy* 26(7):1165–1175. [https://doi.org/10.1175/1520-0485\(1996\)026%28\\$1165:DAISVI%28\\$2.0.CO;2](https://doi.org/10.1175/1520-0485(1996)026%28$1165:DAISVI%28$2.0.CO;2)
- 586 Chang P, Ji L, Li H (1997) A decadal climate variation in the tropical atlantic  
587 ocean from thermodynamic air-sea interactions. *Nature* 385(6616):516–518.  
588 <https://doi.org/10.1038/385516a0>

- 589 Chang P, Yamagata T, Schopf P, et al (2006) Climate fluctuations of tropical  
590 coupled systems—The role of ocean dynamics. *Journal of Climate*  
591 19(20):5122–5174. <https://doi.org/10.1175/JCLI3903.1>
- 592 Cherchi A, Fogli PG, Lovato T, et al (2019) Global mean climate and  
593 main patterns of variability in the cmcc-cm2 coupled model. *Journal of*  
594 *Advances in Modeling Earth Systems* 11(1):185–209. [https://doi.org/10.](https://doi.org/10.1029/2018MS001369)  
595 [1029/2018MS001369](https://doi.org/10.1029/2018MS001369)
- 596 Chiang JC, Vimont DJ (2004) Analogous pacific and atlantic meridional modes  
597 of tropical atmosphere–ocean variability. *Journal of Climate* 17(21):4143–  
598 4158. <https://doi.org/10.1175/JCLI4953.1>
- 599 Chiang JC, Kushnir Y, Giannini A (2002) Deconstructing atlantic intertrop-  
600 ical convergence zone variability: Influence of the local cross-equatorial sea  
601 surface temperature gradient and remote forcing from the eastern equato-  
602 rial pacific. *Journal of Geophysical Research: Atmospheres* 107(D1):ACL–3.  
603 <https://doi.org/10.1029/2000JD000307>
- 604 Contzen J, Dickhaus T, Lohmann G (2021) Variability and extremes: Statisti-  
605 cal validation of the awi-esm. *Geoscientific Model Development Discussions*  
606 pp 1–19. <https://doi.org/10.5194/gmd-2021-225>
- 607 Deppenmeier AL, Haarsma RJ, Hazeleger W (2016) The Bjerknes Feedback  
608 in the Tropical Atlantic in CMIP5 models. *Climate Dynamics* 47(7-8):2691–  
609 2707. <https://doi.org/10.1007/s00382-016-2992-z>
- 610 Deser C, Alexander MA, Xie SP, et al (2010) Sea surface temperature variabil-  
611 ity: Patterns and mechanisms. *Annual review of marine science* 2:115–143.  
612 <https://doi.org/10.1146/annurev-marine-120408-151453>
- 613 Ding H, Keenlyside NS, Latif M (2010) Equatorial Atlantic interannual vari-  
614 ability: Role of heat content. *Journal of Geophysical Research: Oceans*  
615 115(C9). <https://doi.org/10.1029/2010JC006304>
- 616 Dippe T, Lübbecke J, Greatbatch R (2019) A Comparison of the Atlantic  
617 and Pacific Bjerknes Feedbacks: Seasonality, Symmetry, and Stationar-  
618 ity. *Journal of Geophysical Research: Oceans* 124. [https://doi.org/10.1029/](https://doi.org/10.1029/2018JC014700)  
619 [2018JC014700](https://doi.org/10.1029/2018JC014700)
- 620 Doi T, Tozuka T, Yamagata T (2009) Interannual variability of the guinea  
621 dome and its possible link with the atlantic meridional mode. *Climate*  
622 *dynamics* 33(7-8):985–998. <https://doi.org/10.1007/s00382-009-0574-z>
- 623 Döscher R, Acosta M, Alessandri A, et al (2021) The ec-earth3 earth system  
624 model for the climate model intercomparison project 6. *Geoscientific Model*  
625 *Development Discussions* pp 1–90. <https://doi.org/10.5194/gmd-2020-446>

- 626 Eyring V, Bony S, Meehl GA, et al (2016) Overview of the Coupled Model  
627 Intercomparison Project Phase 6 (CMIP6) experimental design and organi-  
628 zation. *Geoscientific Model Development* 9(5):1937–1958. [https://doi.org/  
629 10.5194/gmd-9-1937-2016](https://doi.org/10.5194/gmd-9-1937-2016)
- 630 Foltz GR, McPhaden MJ, Lumpkin R (2012) A strong atlantic meridional  
631 mode event in 2009: The role of mixed layer dynamics. *Journal of Climate*  
632 25(1):363–380. <https://doi.org/10.1175/JCLI-D-11-00150.1>
- 633 Frajka-Williams E, Beaulieu C, Duchez A (2017) Emerging negative atlantic  
634 multidecadal oscillation index in spite of warm subtropics. *Scientific Reports*  
635 7(1):1–8. <https://doi.org/10.1038/s41598-017-11046-x>
- 636 Giannini A, Saravanan R, Chang P (2003) Oceanic Forcing of Sahel Rainfall  
637 on Interannual to Interdecadal Time Scales. *Science* 302(5647):1027–1030.  
638 <https://doi.org/10.1126/science.1089357>
- 639 Golaz JC, Caldwell PM, Van Roekel LP, et al (2019) The doe e3sm coupled  
640 model version 1: Overview and evaluation at standard resolution. *Journal*  
641 *of Advances in Modeling Earth Systems* 11(7):2089–2129. [https://doi.org/  
642 10.1029/2019MS001766](https://doi.org/10.1029/2019MS001766)
- 643 Hu ZZ, Kumar A, Ren HL, et al (2013) Weakened interannual variability in  
644 the tropical pacific ocean since 2000. *Journal of Climate* 26(8):2601–2613.  
645 <https://doi.org/10.1175/JCLI-D-12-00265.1>
- 646 Huang B, Thorne PW, Banzon VF, et al (2017) Extended reconstructed  
647 sea surface temperature, version 5 (ERSSTv5): upgrades, validations, and  
648 intercomparisons. *Journal of Climate* 30(20):8179–8205. [https://doi.org/10.  
649 1175/JCLI-D-16-0836.1](https://doi.org/10.1175/JCLI-D-16-0836.1)
- 650 Keenlyside NS, Latif M (2007) Understanding Equatorial Atlantic Interan-  
651 nual Variability. *Journal of Climate* 20(1):131–142. [https://doi.org/10.1175/  
652 JCLI3992.1](https://doi.org/10.1175/JCLI3992.1)
- 653 Kelley M, Schmidt GA, Nazarenko LS, et al (2020) Giss-e2. 1: Configura-  
654 tions and climatology. *Journal of Advances in Modeling Earth Systems*  
655 12(8):e2019MS002,025. <https://doi.org/10.1029/2019MS002025>
- 656 Kiss AE, Hogg AM, Hannah N, et al (2020) Access-om2 v1. 0: A global  
657 ocean–sea ice model at three resolutions. *Geoscientific Model Development*  
658 13(2):401–442. <https://doi.org/10.5194/gmd-13-401-2020>
- 659 Lauritzen PH, Nair RD, Herrington A, et al (2018) Ncar release of cam-se in  
660 cesm2. 0: A reformulation of the spectral element dynamical core in dry-  
661 mass vertical coordinates with comprehensive treatment of condensates and  
662 energy. *Journal of Advances in Modeling Earth Systems* 10(7):1537–1570.

- 663 <https://doi.org/10.1029/2017MS001257>
- 664 Li L, Yu Y, Tang Y, et al (2020) The flexible global ocean-atmosphere-land  
665 system model grid-point version 3 (fgoals-g3): description and evaluation.  
666 *Journal of Advances in Modeling Earth Systems* 12(9):e2019MS002,012.  
667 <https://doi.org/10.1029/2019MS002012>
- 668 Lin Y, Huang X, Liang Y, et al (2020) Community integrated earth sys-  
669 tem model (ciesm): Description and evaluation. *Journal of Advances in*  
670 *Modeling Earth Systems* 12(8):e2019MS002,036. [https://doi.org/10.1029/](https://doi.org/10.1029/2019MS002036)  
671 [2019MS002036](https://doi.org/10.1029/2019MS002036)
- 672 Liu HL, Bardeen CG, Foster BT, et al (2018) Development and validation  
673 of the whole atmosphere community climate model with thermosphere and  
674 ionosphere extension (waccm-x 2.0). *Journal of Advances in Modeling Earth*  
675 *Systems* 10(2):381–402. <https://doi.org/10.1002/2017MS001232>
- 676 Losada T, Rodríguez-Fonseca B, Janicot S, et al (2010) A multi-  
677 model approach to the Atlantic Equatorial Mode: impact on the West  
678 African Monsoon. *Climate Dynamics* 35(1):29–43. [https://doi.org/10.1007/](https://doi.org/10.1007/s00382-009-0625-5)  
679 [s00382-009-0625-5](https://doi.org/10.1007/s00382-009-0625-5)
- 680 Lübbecke JF, McPhaden MJ (2014) Assessing the twenty-first-century shift in  
681 enso variability in terms of the bjerknes stability index. *Journal of Climate*  
682 27(7):2577–2587. <https://doi.org/10.1175/JCLI-D-13-00438.1>
- 683 Lübbecke JF, Rodríguez-Fonseca B, Richter I, et al (2018) Equatorial Atlantic  
684 variability—Modes, mechanisms, and global teleconnections. *Wiley Interdis-*  
685 *ciplinary Reviews: Climate Change* 9(4):e527. [https://doi.org/10.1002/wcc.](https://doi.org/10.1002/wcc.527)  
686 [527](https://doi.org/10.1002/wcc.527)
- 687 Mahajan S, Saravanan R, Chang P (2010) Free and forced variability of the  
688 tropical atlantic ocean: Role of the wind–evaporation–sea surface temper-  
689 ature feedback. *Journal of climate* 23(22):5958–5977. [https://doi.org/10.](https://doi.org/10.1175/2010JCLI3304.1)  
690 [1175/2010JCLI3304.1](https://doi.org/10.1175/2010JCLI3304.1)
- 691 Mamalakis A, Randerson JT, Yu JY, et al (2021) Zonally contrasting shifts of  
692 the tropical rain belt in response to climate change. *Nature Climate Change*  
693 11(2):143–151. <https://doi.org/10.1038/s41558-020-00963-x>
- 694 Martín-Rey M, Lazar A (2019) Is the boreal spring tropical atlantic variability  
695 a precursor of the equatorial mode? *Climate Dynamics* 53(3):2339–2353.  
696 <https://doi.org/10.1007/s00382-019-04851-9>
- 697 Martín-Rey M, Polo I, Rodríguez-Fonseca B, et al (2018) Is there evidence  
698 of changes in tropical atlantic variability modes under amo phases in the  
699 observational record? *Journal of Climate* 31(2):515–536. <https://doi.org/10.1175/JCLI-D-17-0701.1>

700 [1175/JCLI-D-16-0459.1](https://doi.org/10.1175/JCLI-D-16-0459.1)

701 Martín-Rey M, Polo I, Rodríguez-Fonseca B, et al (2019) Ocean dynamics  
702 shapes the structure and timing of atlantic equatorial modes. *Journal of*  
703 *Geophysical Research: Oceans* 124(11):7529–7544. [https://doi.org/10.1029/](https://doi.org/10.1029/2019JC015030)  
704 [2019JC015030](https://doi.org/10.1029/2019JC015030)

705 Moreno-Chamarro E, Marshall J, Delworth T (2020) Linking itcz migrations  
706 to the amoc and north atlantic/pacific sst decadal variability. *Journal of*  
707 *Climate* 33(3):893–905. <https://doi.org/10.1175/JCLI-D-19-0258.1>

708 Müller WA, Jungclaus JH, Mauritsen T, et al (2018) A higher-resolution  
709 version of the max planck institute earth system model (mpi-esm1. 2-hr).  
710 *Journal of Advances in Modeling Earth Systems* 10(7):1383–1413. <https://doi.org/10.1029/2017MS001217>  
711

712 Nnamchi H, Li J, Kucharski F, et al (2015) Thermodynamic controls of  
713 the Atlantic Niño. *Nature Communications* 6. [https://doi.org/10.1038/](https://doi.org/10.1038/ncomms9895)  
714 [ncomms9895](https://doi.org/10.1038/ncomms9895)

715 Nnamchi HC, Latif M, Keenlyside NS, et al (2020) A satellite era warming hole  
716 in the equatorial atlantic ocean. *Journal of Geophysical Research: Oceans*  
717 125(4):e2019JC015,834. <https://doi.org/10.1029/2019JC015834>

718 Nobre P, Shukla J (1996) Variations of sea surface temperature, wind  
719 stress, and rainfall over the tropical atlantic and south america. *Jour-*  
720 *nal of climate* 9(10):2464–2479. [https://doi.org/10.1175/1520-0442\(1996\)](https://doi.org/10.1175/1520-0442(1996)009$($2464:VOSSTW$)2.0.CO;2)  
721 [009\\$\(\\$2464:VOSSTW\\$\)2.0.CO;2](https://doi.org/10.1175/1520-0442(1996)009$($2464:VOSSTW$)2.0.CO;2)

722 Patricola CM, Saravanan R, Chang P (2014) The impact of the El Niño–  
723 Southern Oscillation and Atlantic meridional mode on seasonal Atlantic  
724 tropical cyclone activity. *Journal of Climate* 27(14):5311–5328. [https://doi.](https://doi.org/10.1175/JCLI-D-13-00687.1)  
725 [org/10.1175/JCLI-D-13-00687.1](https://doi.org/10.1175/JCLI-D-13-00687.1)

726 Pontes G, Wainer I, Prado L, et al (2020a) Reduced atlantic variability  
727 in the mid-pliocene. *Climatic Change* 160(3):445–461. [https://doi.org/10.](https://doi.org/10.1007/s10584-020-02675-9)  
728 [1007/s10584-020-02675-9](https://doi.org/10.1007/s10584-020-02675-9)

729 Pontes GM, Wainer I, Taschetto AS, et al (2020b) Drier tropical and subtropi-  
730 cal southern hemisphere in the mid-pliocene warm period. *Scientific reports*  
731 10(1):1–11. <https://doi.org/10.1038/s41598-020-68884-5>

732 Prigent A, Lübbecke JF, Bayr T, et al (2020) Weakened sst variability in  
733 the tropical atlantic ocean since 2000. *Climate Dynamics* 54(5):2731–2744.  
734 <https://doi.org/10.1007/s00382-020-05138-0>

- 735 Prodhomme C, Voltaire A, Exarchou E, et al (2019) How does the sea-  
736 sonal cycle control equatorial atlantic interannual variability? *Geophysical*  
737 *Research Letters* 46(2):916–922. <https://doi.org/10.1029/2018GL080837>
- 738 Reid PC, Hari RE, Beaugrand G, et al (2016) Global impacts of the 1980s  
739 regime shift. *Global change biology* 22(2):682–703. [https://doi.org/10.1111/  
740 gcb.13106](https://doi.org/10.1111/gcb.13106)
- 741 Richter I, Tokinaga H (2020) An overview of the performance of cmip6 models  
742 in the tropical atlantic: mean state, variability, and remote impacts. *Climate*  
743 *Dynamics* 55(9):2579–2601. <https://doi.org/10.1007/s00382-020-05409-w>
- 744 Richter I, Xie SP (2008) On the origin of equatorial atlantic biases in coupled  
745 general circulation models. *Climate Dynamics* 31(5):587–598. [https://doi.  
746 org/10.1007/s00382-008-0364-z](https://doi.org/10.1007/s00382-008-0364-z)
- 747 Richter I, Behera SK, Masumoto Y, et al (2013) Multiple causes of interannual  
748 sea surface temperature variability in the equatorial Atlantic Ocean. *Nature*  
749 *Geoscience* 6(3):43. <https://doi.org/10.1038/ngeo1660>
- 750 Saha S, Moorthi S, Pan HL, et al (2010) The NCEP climate forecast system  
751 reanalysis. *Bulletin of the American Meteorological Society* 91(8):1015–1058.  
752 <https://doi.org/10.1175/2010BAMS3001.1>
- 753 Schneider T, Bischoff T, Haug GH (2014) Migrations and dynamics of the  
754 intertropical convergence zone. *Nature* 513(7516):45–53. [https://doi.org/10.  
755 1038/nature13636](https://doi.org/10.1038/nature13636)
- 756 S  f  rian R, Nabat P, Michou M, et al (2019) Evaluation of cnrm earth  
757 system model, cnrm-esm2-1: Role of earth system processes in present-  
758 day and future climate. *Journal of Advances in Modeling Earth Systems*  
759 11(12):4182–4227. <https://doi.org/10.1029/2019MS001791>
- 760 Seland  , Bentsen M, Oliv   D, et al (2020) Overview of the norwe-  
761 gian earth system model (noresm2) and key climate response of cmip6  
762 deck, historical, and scenario simulations. *Geoscientific Model Development*  
763 13(12):6165–6200. <https://doi.org/10.5194/gmd-13-6165-2020>
- 764 Sellar AA, Jones CG, Mulcahy JP, et al (2019) Ukesm1: Description and evalu-  
765 ation of the uk earth system model. *Journal of Advances in Modeling Earth*  
766 *Systems* 11(12):4513–4558. <https://doi.org/10.1029/2019MS001739>
- 767 Semmler T, Danilov S, Rackow T, et al (2018) Awi-cm-1.1-mr model output  
768 prepared for cmip6 cmip: links to 1pctco2, abrupt-4xco2, historical, and  
769 piconrol simulations. Earth System Grid Federation

- 770 Servain J (1991) Simple climatic indices for the tropical atlantic ocean and  
771 some applications. *Journal of Geophysical Research: Oceans* 96(C8):15,137–  
772 15,146. <https://doi.org/10.1029/91JC01046>
- 773 Servain J, Caniaux G, Kouadio YK, et al (2014) Recent climatic trends in the  
774 tropical atlantic. *Climate Dynamics* 43(11):3071–3089. <https://doi.org/10.1007/s00382-014-2168-7>  
775
- 776 Silva P, Wainer I, Khodri M (2021) Changes in the equatorial mode of the Trop-  
777 ical Atlantic in terms of the Bjerknes Feedback Index. *Climate Dynamics*  
778 56(9):3005–3024. <https://doi.org/10.1007/s00382-021-05627-w>
- 779 Subramaniam A, Mahaffey C, Johns W, et al (2013) Equatorial upwelling  
780 enhances nitrogen fixation in the Atlantic Ocean. *Geophysical Research*  
781 *Letters* 40(9):1766–1771. <https://doi.org/10.1002/grl.50250>
- 782 Sutton R, Jewson S, Rowell D (2000) The elements of climate variability in  
783 the tropical Atlantic region. *Journal of Climate* 13(18):3261–3284. [https://doi.org/10.1175/1520-0442\(2000\)013%3261:TEOCVI%20.0.CO;2](https://doi.org/10.1175/1520-0442(2000)013%3261:TEOCVI%20.0.CO;2)  
784
- 785 Swart NC, Cole JN, Kharin VV, et al (2019) The canadian earth sys-  
786 tem model version 5 (canesm5. 0.3). *Geoscientific Model Development*  
787 12(11):4823–4873. <https://doi.org/10.5194/gmd-12-4823-2019>
- 788 Tegen I, Neubauer D, Ferrachat S, et al (2019) The global aerosol–climate  
789 model echem6. 3–ham2. 3–part 1: Aerosol evaluation. *Geoscientific model*  
790 *development* 12(4):1643–1677. <https://doi.org/10.5194/gmd-12-1643-2019>
- 791 Tian B, Dong X (2020) The double-itzc bias in cmip3, cmip5, and cmip6  
792 models based on annual mean precipitation. *Geophysical Research Letters*  
793 47(8):e2020GL087,232. <https://doi.org/10.1029/2020GL087232>
- 794 Tokinaga H, Xie SP (2011) Weakening of the equatorial Atlantic cold tongue  
795 over the past six decades. *Nature Geoscience* 4(4):222–226. <https://doi.org/10.1038/ngeo1078>  
796
- 797 Veiga SF, Giarolla E, Nobre P, et al (2020) Analyzing the influence of the  
798 north atlantic ocean variability on the atlantic meridional mode on decadal  
799 time scales. *Atmosphere* 11(1):3. <https://doi.org/10.3390/atmos11010003>
- 800 Vimont DJ, Kossin JP (2007) The Atlantic meridional mode and hurri-  
801 cane activity. *Geophysical Research Letters* 34(7). <https://doi.org/10.1029/2007GL029683>  
802
- 803 Voldoire A, Saint-Martin D, Sénési S, et al (2019) Evaluation of cmip6 deck  
804 experiments with cnrm-cm6-1. *Journal of Advances in Modeling Earth*  
805 *Systems* 11(7):2177–2213. <https://doi.org/10.1029/2019MS001683>

- 806 Volodin E, Mortikov E, Gritsun A, et al (2019) Inm inm-cm5-0 model output  
807 prepared for cmip6 cmip. <https://doi.org/10.22033/ESGF/CMIP6.1423>
- 808 Wu T, Lu Y, Fang Y, et al (2019) The beijing climate center climate  
809 system model (bcc-csm): The main progress from cmip5 to cmip6. *Geo-*  
810 *scientific Model Development* 12(4):1573–1600. [https://doi.org/10.5194/](https://doi.org/10.5194/gmd-12-1573-2019)  
811 [gmd-12-1573-2019](https://doi.org/10.5194/gmd-12-1573-2019)
- 812 Wyser K, Noije Tv, Yang S, et al (2020) On the increased climate sensitivity in  
813 the ec-earth model from cmip5 to cmip6. *Geoscientific Model Development*  
814 13(8):3465–3474. <https://doi.org/10.5194/gmd-13-3465-2020>
- 815 Xiao-Ge X, Tong-Wen W, Jie ZHANG FZ, et al (2019) Introduction of bcc  
816 models and its participation in cmip6. *Advances in Climate Change Research*  
817 15(5):533
- 818 Xie SP, Carton JA (2004) Tropical Atlantic Variability: Patterns, Mechanisms,  
819 and Impacts, American Geophysical Union (AGU), pp 121–142. [https://doi.](https://doi.org/10.1029/147GM07)  
820 [org/10.1029/147GM07](https://doi.org/10.1029/147GM07)
- 821 Xie SP, Philander SGH (1994) A coupled ocean-atmosphere model of relevance  
822 to the itcz in the eastern pacific. *Tellus A* 46(4):340–350. [https://doi.org/](https://doi.org/10.1034/j.1600-0870.1994.t01-1-00001.x)  
823 [10.1034/j.1600-0870.1994.t01-1-00001.x](https://doi.org/10.1034/j.1600-0870.1994.t01-1-00001.x)
- 824 Xie SP, Deser C, Vecchi GA, et al (2010) Global warming pattern formation:  
825 Sea surface temperature and rainfall. *Journal of Climate* 23(4):966–986.  
826 <https://doi.org/10.1175/2009JCLI3329.1>
- 827 Yang Y, Wu L, Guo Y, et al (2021) Greenhouse warming intensifies north  
828 tropical atlantic climate variability. *Science advances* 7(35):eabg9690. [https:](https://doi.org/10.1126/sciadv.abg9690)  
829 [//doi.org/10.1126/sciadv.abg9690](https://doi.org/10.1126/sciadv.abg9690)
- 830 Zebiak SE (1993) Air–Sea Interaction in the Equatorial Atlantic Region. *Jour-*  
831 *nal of Climate* 6(8):1567–1586. [https://doi.org/10.1175/1520-0442\(1993\)](https://doi.org/10.1175/1520-0442(1993)006$($1567:AIITEA$)2.0.CO;2)  
832 [006\\$\(\\$1567:AIITEA\\$\)2.0.CO;2](https://doi.org/10.1175/1520-0442(1993)006$($1567:AIITEA$)2.0.CO;2)
- 833 Zhang W, Vecchi GA, Villarini G, et al (2017) Modulation of western North  
834 Pacific tropical cyclone activity by the Atlantic Meridional Mode. *Climate*  
835 *Dynamics* 48(1-2):631–647. <https://doi.org/10.1007/s00382-016-3099-2>
- 836 Ziehn T, Chamberlain MA, Law RM, et al (2020) The australian earth sys-  
837 tem model: Access-esm1. 5. *Journal of Southern Hemisphere Earth Systems*  
838 *Science* 70(1):193–214. <https://doi.org/10.1071/ES19035>

## Supplementary Files

This is a list of supplementary files associated with this preprint. Click to download.

- [draft2IOA1variabilityclimatedynamicssupinfo.pdf](#)